Author's copy. To appear in Computer Graphics Forum, 2016

Eurographics Conference on Visualization (EuroVis) 2016
K.-L. Ma, G. Santucci, and J. van Wijk
(Guest Editors)

Volume 35 (2016), Number 3

Space-Time Bifurcation Lines for Extraction of 2D Lagrangian Coherent Structures

Gustavo Machado[1], Sebastian Boblest[2], Thomas Ertl[2], and Filip Sadlo[3]

[1] Federal University of Santa Catarina, Brasil
[2] University of Stuttgart, Germany
[3] Heidelberg University, Germany

Abstract

We present a novel and efficient technique to extract Lagrangian coherent structures in two-dimensional time-dependent vector fields. We show that this can be achieved by employing bifurcation line extraction in the space-time representation of the vector field, and generating space-time bifurcation manifolds therefrom. To show the utility and applicability of our approach, we provide an evaluation of existing extraction techniques for Lagrangian coherent structures, and compare them to our approach.

Categories and Subject Descriptors (according to ACM CCS): Simulation and Modeling [I.6.6]: Simulation Output Analysis—; Physical Sciences and Engineering [J.2]: Physics—

1. Introduction

Lagrangian coherent structures (LCS) are nowadays a widely-applied approach to the extraction of the topological structure of time-dependent vector fields. These structures act as barriers over finite time scopes and thus provide insight into mixing behavior and transport in general. The probably most widely-used approach to extract LCS is by computation of the finite-time Lyapunov exponent (FTLE) field [Hal01], followed by ridge extraction (Figure 1(a)). Several approaches have been proposed for the extraction of ridges in this context, including c-ridges [SPFT12], and second-derivative ridges [SLM05], while height ridges [Ebe96] seem to be most widely employed.

Because the computation of a single time instance of the FTLE field requires the integration of a trajectory, i.e., a pathline, for each of its sample points, acceleration strategies have been proposed based on adaptive sampling [GGTH07, SP07] for single time steps of the FTLE field, and on grid advection [SRP11] for time series, i.e., animations. While these concepts still extract LCS by means of a purely geometric approach, i.e., by extracting ridges from the FTLE field, it has been shown that traditional vector field topology [Asi93, HH89] can be generalized to time-dependent vector fields by replacing streamlines with streaklines in the concept [SW10, USE13], resulting in a topological approach in the original sense from dynamical systems theory.

The concept central to the streak-based approaches are so-called hyperbolic trajectories (HT); those are trajectories in the hyperbolic regime of a vector field toward which, for locally the longest time, other trajectories converge in forward and reverse time [Hal00] (Figure 1(c)). LCS can be obtained by seeding trajectories along HTs in space and time, in other words, by seeding streaklines along hyperbolic trajectories in 2D [SW10] and streaksurfaces along hyperbolic path surfaces in 3D [USE13].

A major difficulty with this approach is, however, that hyperbolic trajectories are particularly difficult to integrate because in either direction, forward or reverse, there is a respective LCS that repels them and thus causes exponential error growth (Figure 2(b)). Practically, this results in the problem of computing FTLE fields both with forward and reverse advection in an adaptive sampling manner that refines the fields at the intersection of the respective forward and reverse LCS, to obtain intersections of sufficient accuracy. The intersection point (e.g., at t_0 in Figure 1(b)) then serves as the seed for a pathline whose hyperbolic part is the HT. Nevertheless, because of the error growth, the longer the HT that has to be extracted, the more accurately the LCS intersection has to be determined, leading to an increase in computational cost. On the other hand, once a HT has been extracted, the computation of the streak manifolds from it is typically much less expensive than computing the FTLE field for each time step and extracting height ridges therefrom. It has been shown that the streak-based approach is thus faster, in particular when generating time series (animations) of the FTLE field, and at the same time tends to be even more accurate [USE13].

The utility of HTs is not constrained to LCS extraction. They provide a concise representation [BSDW12], i.e., the skeleton of time-dependent vector field topology, and help understand the hyperbolic dynamics that cause the topological structure of vector fields. Bachthaler et al. [BSDW12, SBDW13] extract LCS by height ridge surface extraction in space-time. While this approach suffers from computational cost, because the FTLE field needs to be computed for each instant of time within the considered time interval, it provides globally accurate HTs by means of the intersection curves of the space-time ridge surfaces of the forward and reverse FTLE fields (Figure 1(b)).

In this paper, we show that the problem of extracting HTs together with their manifolds (LCS) from 2D time-dependent vector fields is equivalent to extracting bifurcation lines [PC87, MSE13] and their manifolds in the corresponding 3D space-time vector field. Although this contribution is rather theoretical, i.e., we employ an existing technique (bifurcation line/manifold extraction) in a derived field (space-time vector field), we show that it has a high impact because:

- The extraction of LCS based on space-time bifurcation lines is substantially faster than previous approaches,
- the involved extraction of HTs is not subject to exponential error growth, and
- because we free the streakline-based topology concept from the necessity of computing FTLE fields, it results in a formulation that is even closer to the traditional formulation of vector field topology based on streamlines, i.e., the seeding structure is defined locally. In this sense, the extraction of bifurcation lines in space-time represents the direct time-dependent counterpart to the extraction of saddle-type critical points.

We validate our novel approach with the results from the streakline-based topology paper [SW10]. Beyond this, we show that separation lines and attachment lines at no-slip boundaries also represent hyperbolic trajectories and thus have to be included in topological analysis. We complement our theoretical contributions with an evaluation and comparison with previous approaches for LCS extraction.

2. Related Work and Fundamentals

We give an introduction to the closely related research fields and bring them into context with our technique.

Traditional Topology and Time Dependence A good introduction to traditional 2D vector field topology, i.e., based on *streamlines* and thus applicable to instantaneous/steady vector fields only, is provided by Asimov [Asi93] and Helman and Hesselink [HH89].

Different approaches have been proposed so far for vector field topology alternatives that are able to capture the topology of time-dependent vector fields. Pobitzer et al. [PPF*11] provide an introduction to this field. Kasten et al. [KHNH10], and Fuchs et al. [FKS*10] investigate time-dependent counterparts to critical points. These approaches can be seen as complementary to the approaches based on hyperbolic trajectories [Hal00, SW10, USE13]. Kasten et al. build on acceleration while Fuchs et al. introduce an unsteadiness measure. Theisel et al. [TWHS04] presented an early approach based on streamlines and pathlines, that has not yet been compared with FTLE-related approaches. Regarding the utilization of space-time concepts in flow visualization, Theisel and Seidel [TS03] present a derived field called feature flow field. Coming from the opposite direction, Chen et al. [CKW*12] use topological methods to design 2D time-dependent vector fields.

Lagrangian Coherent Structures from FTLE The lack of a vector field topology concept for time-dependent vector fields led to the proposition of different approaches during the last decade, out of which concepts based on (or consistent with) the FTLE field attracted special attention. The FTLE is obtained from characteristic curves of type *pathline*, making it appropriate for time-dependent vector fields

$$\mathbf{u}(\mathbf{x},t) = \Big(u(x,y,t),\, v(x,y,t)\Big)^{\top} \tag{1}$$

with $\mathbf{x} = (x,y)^{\top}$. A pathline is conceptually seeded at each sample point and the distance between the end points of neighboring pathlines of advection time T constitutes the essential quantity reflected by the FTLE. In detail, the FTLE field $\sigma_{t_0}^{T}(\mathbf{x})$ at position $\mathbf{x}$, time t_0, and for advection time T is typically computed as

$$\sigma_{t_0}^{T}(\mathbf{x}) = \frac{1}{|T|} \ln \sqrt{\lambda_{\max}\left(\left(\nabla \boldsymbol{\phi}_{t_0}^{T}(\mathbf{x})\right)^{\top} \nabla \boldsymbol{\phi}_{t_0}^{T}(\mathbf{x})\right)}, \tag{2}$$

where $\boldsymbol{\phi}_{t_0}^{T}(\mathbf{x})$ represents the *flow map* that maps the seed point $\mathbf{x}$ of a pathline started at time t_0 to its end point $\boldsymbol{\phi}_{t_0}^{T}(\mathbf{x})$ after integration time T (Figure 1(a)), and $\lambda_{\max}(\cdot)$ is the major eigenvalue. We refer the reader to Haller [Hal01] for a thorough introduction to the finite-time Lyapunov exponent.

Ridges in $\sigma_{t_0}^{T}(\mathbf{x})$ for $T < 0$ represent *attracting LCS*, i.e., particles are attracted to these manifolds in forward time, while ridges in $\sigma_{t_0}^{T}(\mathbf{x})$ for $T > 0$ represent *repelling LCS* (Figure 1(c)) where particles are attracted in reverse time. Ridge extraction from the FTLE is comparably easy to employ, but it exhibits several downsides. The most hindering problems include: very strong aliasing [USK*12] (Figure 1(d) and (e)), which can impede extraction of ridges, the requirement of problem-dependent and often not globally feasible advection times T [SLM05, SUEW12, Sad15], and the computationally very expensive computation of the FTLE. Although several acceleration techniques have been proposed so far for the computation of FTLE (time series) [GGTH07, SP07, SRP11, HSW11], the achieved overall accelerations are moderate because still comparably many samples are required.

A further drawback is the implicit nature of this LCS definition. Traditional vector field topology is defined in terms of special streamlines—those that degenerate to points because they are started at isolated points where the vector field is zero are called *critical points*, and those that converge to critical points of type saddle (i.e., hyperbolic critical points) either in forward or reverse time are called *separatrices*, because they separate regions of qualitatively different behavior of the vector field. In this respect, traditional vector field topology is defined by an explicit generating rule: saddle-type critical points represent the locally obtained seeds, and separatrices are grown from these seeds in forward and reverse time using streamlines. In contrast, FTLE-based LCS extraction needs to compute the FTLE field within the entire domain with costly integration and then the LCS are extracted from the FTLE field ridge extraction on a purely geometrical (local) basis, including all the problems typical for feature extraction such as false negatives and false positives. This approach is intrinsically implicit: it lacks a respective generating rule. Additionally, since the FTLE needs to be sampled prior to knowledge of the location of the LCS, and because LCS are extremely thin structures in the FTLE field, the

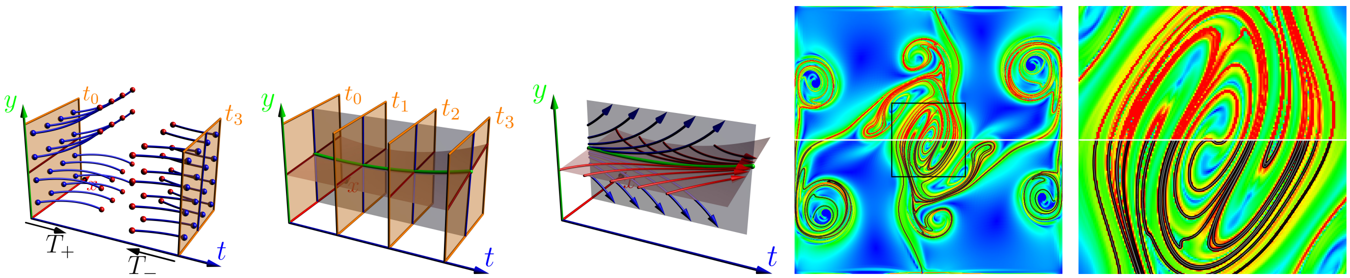

(a) (b) (c) (d) (e)

Figure 1: *(a) Forward-time (T_+) FTLE computation with ridge (red curve on orange sampling plane at t_0), and reverse-time (T_-) FTLE with ridge (blue curve at t_3). (b) A dense space-time stack of FTLE fields reveals space-time ridge surface (forward-time red, reverse-time blue). The intersection of forward and reverse space-time ridge surface yields the hyperbolic trajectory (space-time bifurcation line, green). (c) Repelling LCS / stable bifurcation manifold (red), and attracting LCS / unstable bifurcation manifold (blue) of bifurcation line (green). (d) Upper half: FTLE suffers from sampling issues (Buoyant Plumes dataset, cf. Section 5.3 and Figure 4(d)) and provides only an implicit determination of LCS. Lower half: Our streakline manifolds (black curves), in contrast, capture the LCS at high accuracy and are not subject to aliasing. (e) Close-up of region (black box) indicated in (d).*

approach suffers from severe sampling issues (Figure 1(d), (e)). This becomes particularly impeding if the FTLE is computed for longer advection times T, since LCS grow with advection time, and if the domain is spatially limited, the LCS undergo folding and stretching. This results in very finely folded and arbitrarily closely adjacent LCS that cannot be appropriately sampled with feasible resolutions without a priori information.

Streak-Based Topology Motivated by these drawbacks, traditional vector field topology was generalized to time-dependent vector fields by replacing the role of streamlines by characteristic curves of type *streakline* in the concept (note that streamlines and streaklines are identical in steady vector fields), for 2D [SW10], and more recently for 3D [USE13] vector fields. In this approach, LCS are obtained by growing generalized streaklines [WTS*07] from hyperbolic trajectories. The seeds of generalized streaklines are allowed to move over time and, in this concept, they move (advect) along hyperbolic trajectories during streakline generation. As stated by Haller [Hal00], hyperbolic trajectories in 2D vector fields represent pathlines that reside in *hyperbolic regions* for locally the longest time. He defines those regions to be hyperbolic where $\det(\nabla \mathbf{u}(\mathbf{x},t)) < 0$.

The advantages of the streakline-based topology are manifold. Once hyperbolic trajectories are obtained, the streak-based LCS can be grown from them to arbitrary times—dense folding of LCS does not affect the extraction (Figure 1(d), (e)), since streaklines are constructed in a Lagrangian manner, in contrast to FTLE ridges which need to be extracted in the Eulerian frame. Hence, streak-based topology does not suffer from the abovementioned aliasing problems. The resulting streak manifolds are of superior quality [USE13], as they are attracted to the LCS they are representing, at least as long as they are close to the HT. Since attracting LCS are obtained by growing streaklines forward in time, and repelling LCS in reverse time, both get attracted by the respective LCS. Finally, only hyperbolic LCS are obtained, as with Haller's recent approach [Hal11]. For example, shear-induced FTLE ridges, as obtained by FTLE ridge extraction, are usually not considered significant in topological analysis of time-dependent flow. In Section 5.3, we compare the traditional approach based on FTLE ridge extraction with our streak-based approach for some selected examples.

The major shortcomings of Haller's HT-based approach [Hal00] and streak-based topology [SW10, USE13] are, however, with respect to the extraction of the required HTs. To obtain seed points for them, Haller computes the hyperbolicity time field forward and reversely and intersects ridges therefrom, while Sadlo and Weiskopf [SW10, USE13] extract ridges from the forward and reverse FTLE and intersect them. Both approaches are computationally expensive and subject to aliasing. However, the most serious problem of the above approaches is the extraction of the HTs: they require very accurate seed points [SW10, USE13].

LCS in Space-Time As a remedy to this problem, Bachthaler et al. [BSDW12] obtain HTs by intersecting forward and reverse FTLE ridges over the entire time domain (Figure 1(b)). Because they obtain the FTLE ridges over the complete time domain, there is no necessity to generate the LCS by growing streak manifolds from the HT. Instead, they exploit that LCS represent material lines, i.e., that they advect with the flow (up to negligible cross-flux [SLM05]). Using the space-time representation

$$\tilde{\mathbf{u}}(\tilde{\mathbf{x}}) = \Big(u(x,y,t),\, v(x,y,t),\, 1\Big)^{\top}, \tag{3}$$

of the vector field $\mathbf{u}(\mathbf{x},t)$, with $\tilde{\mathbf{x}} = (x,y,t)^{\top}$, and by making use of the fact that streamlines of $\tilde{\mathbf{u}}(\tilde{\mathbf{x}})$ represent pathlines of $\mathbf{u}(\mathbf{x},t)$ and since LCS thus advect along streamlines in $\tilde{\mathbf{u}}(\tilde{\mathbf{x}})$, LCS represent streamsurfaces in $\tilde{\mathbf{u}}(\tilde{\mathbf{x}})$ sufficiently well. This property allowed Bachthaler et al. to apply line integral convolution [CL93] of the $\tilde{\mathbf{u}}(\tilde{\mathbf{x}})$ field on the FTLE ridges to visualize stretching and squeezing within LCS, i.e., in direction tangential to the LCS.

Bifurcation Lines and Separation Lines In 3D steady vector fields, bifurcation lines [PC87, MSE13] (Figure 1(c)) are streamlines that represent asymptotes for other streamlines for locally the longest time, for both forward and reverse integration. As stated by Roth [Rot00], bifurcation lines can be seen as an extension of separation and attachment lines to 3D, in that they represent an attachment line in one manifold, and simultaneously a separation line in another manifold, both intersecting along the bifurcation line.

Separation/attachment lines [Ken98] and bifurcation lines are somewhat difficult to spot. While vortex core lines are, at least from the view of the vortex core line criterion by Sujudi and Haimes [SH95], closely related to bifurcation lines (they can be seen as their complement [MSE13]), vortex core lines are easier to define, e.g., as curves that, at least over intervals of time, represent an individual streamline around which other streamlines spiral. A respective definition is not as easy to give for separation/attachment or bifurcation lines. These lines all exhibit neighboring streamlines that converge or diverge from them, but unfortunately this is, to some extent, also the case for these neighboring streamlines. The most apparent definition for separation/attachment lines is due to Kenwright [Ken98]: if a large set of streamlines is computed, they will tend to merge along separation lines with forward integration, and along attachment lines when integrating in reverse direction. This experiment is the primary way to validate a separation/attachment or bifurcation line. Tricoche et al. [TGS05] use a related approach based on divergence of streamlines to detect lines of attachment and separation. As a consequence, bifurcation lines are streamlines that represent asymptotes for other streamlines, simultaneously in forward and reverse direction (i.e., they also reside in hyperbolic regions), for *locally the longest time* (cf. the analogous definition of HTs above by Haller [Hal00]). In a follow-up paper, Kenwright et al. [KHL99] give the more explicit definition for separation and attachment lines as the loci where velocity $\mathbf{u}$ and a real eigenvector of $\nabla\mathbf{u}$ are (anti)parallel. As stated by Roth [Rot00], this approach provides only the correct curves if the separation or attachment lines are straight. It can be extended to obtain bifurcation lines in 3D, however, with the same limitations.

Machado et al. [MSE13] take the (error-affected) curves from Roth's method [Rot00] or those obtained by the higher-order approach due to Roth and Peikert [RP98] presented originally for curved vortex core lines as initial solution, and refine them toward the aimed asymptotes that represent bifurcation lines.

As a secondary step, they extract the two 2D manifolds of a bifurcation line, the (stable) one consisting of those streamlines that converge to it in forward, and the (unstable) one that consists of streamlines converging to the bifurcation line in reverse time (Figure 1(c)). Similar to separatrix generation from saddle-type critical points, they employ a small offset along the respective eigenvector of $\nabla\mathbf{u}$, projected orthogonally to the curve, to obtain seed curves (one on either side of the bifurcation line for each eigenvector) for integrating streamsurfaces that provide the bifurcation manifolds.

3. LCS by Space-Time Bifurcation Lines

In this paper, we present, to the best of our knowledge, the first technique to obtain hyperbolic trajectories (and thus time-dependent topology) without computing integral curves. Neither do we need to integrate an auxiliary field such as hyperbolicity time [Hal00] or the FTLE [SW10, USE13], nor do we need to employ integration to obtain the hyperbolic trajectories themselves—we extract them as *bifurcation lines* [MSE13] from the space-time field $\tilde{\mathbf{u}}(\tilde{\mathbf{x}})$.

As already mentioned, streamlines of $\tilde{\mathbf{u}}(\tilde{\mathbf{x}})$ in Equation (3) represent pathlines of $\mathbf{u}(\mathbf{x},t)$. Since both bifurcation lines and HTs represent curves that attract the respective type of curves (3D streamlines in the case of bifurcation lines and 2D pathlines in the case of HTs) for locally the longest time in both directions of time, *extracting bifurcation lines from* $\tilde{\mathbf{u}}(\tilde{\mathbf{x}})$ *is identical to extracting hyperbolic trajectories from* $\mathbf{u}(\mathbf{x},t)$. This is the approach central to the present paper. We extract bifurcation lines from $\tilde{\mathbf{u}}(\tilde{\mathbf{x}})$ and compute their streamsurface manifolds also in $\tilde{\mathbf{u}}(\tilde{\mathbf{x}})$, according to the method by Machado et al. [MSE13] that is based on Roth's formulation. As detailed in Figure 1 of Weinkauf and Theisel [WT10], a spatial section of a space-time streamsurface represents a streakline and hence, the space-time bifurcation manifolds represent the streak manifolds in streak-based vector field topology [SW10].

The algorithm [MSE13] for the extraction of bifurcation lines consists of two basic steps: first, an initial solution is inferred (Section 3.1), this solution is the refined toward the feature line (Section 3.2). Algorithm 1 gives a schematic overview of this method.

3.1. Bifurcation Line Candidates

This step is performed based on the parallel vectors operator [PR99], which is defined as the loci where two vector fields $\mathbf{v}$ and $\mathbf{w}$ are parallel (or antiparallel). According to Roth [Rot00] and Machado et al. [MSE13], bifurcation lines can be extracted as the loci where the steady vector field $\mathbf{v}$ is parallel to the steady formulation of acceleration, $\mathbf{a} := (\nabla\mathbf{v})\mathbf{v}$, or to the jerk vector $\mathbf{b} := (\nabla\mathbf{a})\mathbf{v}$. Here, we employ the equivalent to $\mathbf{v} \parallel \mathbf{a}$ but in space-time representation of the 2D time-dependent vector field, i.e., we extract space-time bifurcation lines as the loci where $\tilde{\mathbf{u}} \parallel \tilde{\mathbf{a}}$, with $\tilde{\mathbf{a}} := (\nabla\tilde{\mathbf{u}})\tilde{\mathbf{u}}$, by finding points, where

$$\tilde{\mathbf{u}} \times \tilde{\mathbf{a}} = \mathbf{0}. \tag{4}$$

Note that in our case, with the t-component of $\tilde{\mathbf{u}}$ being constant, Equation (4) directly leads to $\tilde{\mathbf{a}} = \mathbf{0}$ because the t-component of $\tilde{\mathbf{a}}$ vanishes and the t-component of $\tilde{\mathbf{u}}$ is 1:

$$\nabla\tilde{\mathbf{u}} = \begin{pmatrix} u_{,x} & u_{,y} & u_{,t} \\ v_{,x} & v_{,y} & v_{,t} \\ 0 & 0 & 0 \end{pmatrix}, \tilde{\mathbf{a}} = \begin{pmatrix} u_{,x}u + u_{,y}v + u_{,t}1 \\ v_{,x}u + v_{,y}v + v_{,t}1 \\ 0 \end{pmatrix}. \tag{5}$$

It is clear that, in general, the solutions to $\tilde{\mathbf{a}} = \mathbf{0}$ are curves in the (x,y,t)-space as we only have two equations for three variables. This is not surprising, because generally the condition of a vanishing cross product leads to curves in three-dimensional space and not to isolated points [PR99]. To use the technique by Machado et al. [MSE13] without modifications, we decided to employ condition (4). In our experiments, we observed that the solution of $\tilde{\mathbf{u}} \parallel \tilde{\mathbf{b}}$, with $\tilde{\mathbf{b}} := (\nabla\tilde{\mathbf{a}})\tilde{\mathbf{u}}$, which, of course is also equivalent to $\tilde{\mathbf{b}} = \mathbf{0}$ in our case, did not yield satisfactory results. Similar findings were described by Machado et al. for $\mathbf{v} \parallel \mathbf{b}$, i.e., that this condition most of the time gives very accurate results, but also frequently yields false negatives, in contrast to $\mathbf{v} \parallel \mathbf{a}$.

Subsequently, we apply a first *filtering* to reject non (or weakly) hyperbolic parts of $\tilde{\mathbf{u}} \parallel \tilde{\mathbf{a}}$ and obtain the initial solution. This is performed with three user-defined thresholds [MSE13]: minimum strength τ_h, maximum angle τ_α, and minimum length τ_l. For the parts where all three eigenvalues of $\nabla\tilde{\mathbf{u}}$ are real, we project $\nabla\tilde{\mathbf{u}}$

Algorithm 1 Bifurcation line extraction [MSE13].

1: Find all vertices of initial bifurcation line candidate with parallel vectors operator [PR99] (Section 3.1)
2: Apply filtering (minimum strength τ_h, maximum angle τ_α, minimum length τ_l, Section 3.1)
3: **while** Bifurcation line insufficiently accurate **do**
4: Update vertices by reducing $\alpha_i(\boldsymbol{\vartheta}_i, \tilde{\mathbf{u}})$ (Section 3.2)
5: **end while**

Algorithm 2 LCS extraction presented in this work.

1: Create space-time representation of 2D time-dependent vector field (Section 2)
2: Compute bifurcation lines for $\tilde{\mathbf{u}}$ with Algorithm 1
3: Extract LCS by seeding streamsurfaces in $\tilde{\mathbf{u}}$ along bifurcation line [MSE13]

onto a plane perpendicular to the line and compute its determinant d. Hyperbolicity is identified at those points where $d < 0$. To reject parts with low hyperbolicity as well, we require $d/\|\tilde{\mathbf{u}}\| > -\tau_h$. We then reject all parts, where the angle $\alpha(\boldsymbol{\vartheta}, \tilde{\mathbf{u}})$ between the line tangent $\boldsymbol{\vartheta}$ and the vector field $\tilde{\mathbf{u}}$ is larger than the threshold τ_α. Finally, all remaining feature lines that are shorter than τ_l are discarded.

3.2. Iterative Refinement of Candidates

In this step of the algorithm [MSE13], an iterative refinement is employed, that deforms the initial solution toward the actual space-time bifurcation line. To do that, we take each vertex $\mathbf{c}_i$ of the candidate polyline and construct a plane normal to the line at $\mathbf{p}_i = (\mathbf{c}_{i+1} + \mathbf{c}_{i-1})/2$ (at boundary vertices we assume $\mathbf{p}_i = \mathbf{c}_i$) and, inside this plane, we employ a small step in the direction that reduces the angle $\alpha_i(\boldsymbol{\vartheta}_i, \tilde{\mathbf{u}})$ between $\tilde{\mathbf{u}}$ and the line's tangent $\boldsymbol{\vartheta}_i$ at $\mathbf{p}_i$. Thus, at each iteration, we update the position of each vertex of the polyline via

$$\mathbf{c}_i \leftarrow \mathbf{p}_i - \Delta\rho \times \|\nabla\alpha_i(\boldsymbol{\vartheta}_i, \tilde{\mathbf{u}})\|, \tag{6}$$

where $\Delta\rho$ is the step size, which is reduced after each iteration step. Finally, the space-time bifurcation lines are obtained after applying a second threshold filtering with stricter constraints $\tau'_h > \tau_h$, $\tau'_\alpha < \tau_\alpha$, and $\tau'_l > \tau_l$. Algorithm 2 gives a sketch of our method, using Algorithm 1. Please compare this with the method of Sadlo and Weiskopf [SW10] that is lined out in Algorithm 3.

4. Discussion

A somewhat counterintuitive circumstance is that hyperbolic trajectories are streamlines in the space-time vector field $\tilde{\mathbf{u}}(\tilde{\mathbf{x}})$ and that streamlines in $\mathbf{u}(\mathbf{x},t)$ are not Galilean-invariant, while LCS are. Actually, pathlines are Galilean-invariant and streamlines in $\tilde{\mathbf{u}}(\tilde{\mathbf{x}})$ represent pathlines in $\mathbf{u}(\mathbf{x},t)$. A Galilean transformation of $\mathbf{u}(\mathbf{x},t)$ would result in a change of the orientation of the vectors in the $\tilde{\mathbf{u}}(\tilde{\mathbf{x}})$ field. However, at the same time it would warp the domain of $\tilde{\mathbf{u}}(\tilde{\mathbf{x}})$ consistently, due to the influence of the Galilean transformation on the coordinate functions. So, in the end, the pathlines in the transformed $\mathbf{u}(\mathbf{x},t)$ field would again represent streamlines in $\tilde{\mathbf{u}}(\tilde{\mathbf{x}})$, i.e., streamlines in $\tilde{\mathbf{u}}(\tilde{\mathbf{x}})$ are invariant under Galilean transformations.

Algorithm 3 LCS extraction (Sadlo and Weiskopf [SW10]).

1: Compute forward-time FTLE field σ_f and reverse-time FTLE field σ_r (Figure 1(a))
2: **while** FTLE ridge intersection insufficiently accurate **do**
3: Intersect ridges of σ_f and σ_r (Figure 1(b) at t_0)
4: Refine FTLE fields around intersection point
5: **end while**
6: Seed hyperbolic trajectory at computed intersection
7: Seed generalized streak lines along hyperbolic trajectory to extract LCS (Figure 1(c))

From a practical point of view, our approach does not suffer from the integration difficulties of HTs. It can extract them irrespective of their length. Furthermore, it is substantially faster (see Figure 6).

Note that in the previous streak-based approach [SW10], not all intersections between forward and reverse FTLE ridges give rise to hyperbolic trajectories. Pathlines are started at these intersections only if the vector field is hyperbolic there and they are stopped as soon as they leave the hyperbolic region. As described by Machado et al. [MSE13], a bifurcation line has to exhibit hyperbolic behavior in the cross section perpendicular to its tangent as well. Hence, both our approach and the streak-based method [SW10] provide a filtering by hyperbolicity. Note that our "hyperbolicity" is measured in space-time planes while in the approach by Sadlo and Weiskopf [SW10], it is hyperbolicity in space only. But this does not matter, the constituting property why space-time bifurcation lines represent HTs was explained above. The main difference of the two approaches is that the one by Sadlo and Weiskopf [SW10] features T as scale parameter, while our approach, in compliance with traditional vector field topology, does not provide such a parameter. This means that we conceptually obtain even weak or short-termed HT that might not give rise to sufficiently pronounced FTLE ridges for a given T. In our approach, the bifurcation manifolds will not grow away sufficiently from the HT in these cases, providing a quantitative representation of the strength of hyperbolic separation (cf. [USE13]). Note that in compliance with the earlier methods [SW10, MSE13], we provide the user the option to reject regions of HTs that are not sufficiently hyperbolic and subsequently allow for rejecting too short HTs.

During our experiments, we observed that in configurations where the flow attaches to or detaches from the domain boundary (cf. Figure 4), our approach missed the related LCS (e.g., the vertical one in Figure 4). Such configurations represent a "half" of a saddle-type critical point, i.e., in our case a "half" of a space-time bifurcation line. One option would have been to implement space-time extraction of separation and attachment lines, with the refinement [MSE13]. We follow an alternative approach here: we simply strip the outermost layer of nodes at no-slip boundaries to get rid of the layer of zero-velocity, and then mirror a band of cells (in our case we mirrored all nodes that were within a distance of 20 cells to the boundary) with the boundary as symmetry axis. This way, we complete the "half" bifurcation lines to regular bifurcation lines that we can then simply extract with our approach. The top and bottom seeding curves in Figure 4 were obtained this way.

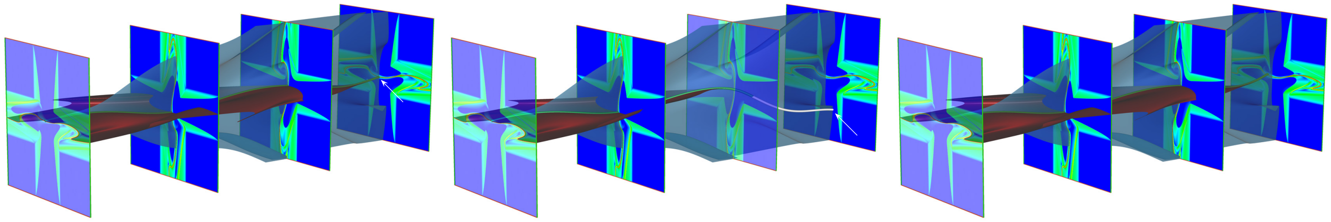

(a) (b) (c)

Figure 2: *Oscillating Gyre-Saddle dataset. (a) Our result by extracting the hyperbolic trajectory (green) as a space-time bifurcation line, with bifurcation manifolds (red, blue) representing the streak manifolds (LCS) of streak-based topology. FTLE slices (red: high, blue: low) from left to right:* $(t_0,T) = (4,5)$, $(6.5,-5)$, $(9,-5)$, *and* $(11.5,5)$. *Our hyperbolic trajectory extraction resides exactly at the intersection (arrow) of the attracting and repelling LCS, in contrast to integration-based extraction [SW10] (b), where errors tend to grow exponentially. There, the deviated white part of the extracted hyperbolic trajectory is located in a non-hyperbolic region, and, hence, it is not suitable there for extraction of streak manifolds. (c) The refinement approach for bifurcation line extraction (Section 3.2) causes a small deformation at both ends. However, this has typically, as in this case, no impact. Nevertheless, we extract longer bifurcation lines and trim them to the region of interest to avoid this.*

4.1. Limitations

The major limitation of our approach lies in the extraction technique for bifurcation lines [MSE13]. As discussed there, it is subject to false negatives, i.e., it may miss bifurcation lines. The technique is based on two extraction criteria for vortex core lines [SH95, RP98], which are both successful in different configurations. Unfortunately, there are cases where both criteria do not provide a solution and hence the bifurcation line is missed.

The second limitation of the bifurcation line extraction technique [MSE13] concerns the ends of bifurcation lines. The approach obtains candidates for bifurcation lines by a modification of vortex core line criteria [SH95, RP98], which are subsequently refined to make them fit a streamline. This refinement performs very well if the bifurcation lines are closed, as in the case of saddle-type periodic orbits. However, if the bifurcation line is open, the refinement phase tends to deform the ends of the extracted line away from the true bifurcation line. This inaccuracy is often negligible because the bifurcation manifolds are attracted to the respective LCS (Figure 2(c)), however, there can be cases where it leads to inaccuracies of the resulting streak manifolds.

Visualization of bifurcation lines is a rather new topic and there is potential for improvement. Future extraction techniques for bifurcation lines can be directly employed in our concept, and hence lower the risk of false negatives or deformed HTs. In the meantime, we recommend to validate the results with selected FTLE slices (as done in our results) or the previous streak-based approach [SW10].

5. Results

In Sections 5.1 and 5.2, we compare our approach to that by Sadlo and Weiskopf [SW10] by applying our technique to one analytic dataset and one from a computational fluid dynamics (CFD) simulation from that paper. Then (Section 5.3), we apply our technique to a CFD dataset used by Bachthaler et al. [BSDW12]. We conclude our results with an evaluation of our approach and the most closely related techniques for LCS extraction (Section 5.4).

5.1. Oscillating Gyre-Saddle

This dataset is derived from Shadden's steady-type Double-Gyre flow and consists of a saddle-type configuration with cosine velocity profile across its "arms" and a fixed angle of $\pi/2$ between its "arms". The saddle translates in an oscillating manner between the locations $(0.25, 0.25)$ and $(-0.25, -0.25)$ at a period of 4 s. This example serves as a test if the concept is able to extract the time-dependent topology of a moving hyperbolic region.

Figure 2(a) shows the result from our approach with the respective attracting LCS at the backmost FTLE slice. It can be seen that our bifurcation line-based extraction of the HT is not affected by the repelling LCS, i.e., it resides also at the backmost FTLE slice at the intersection of the attracting and repelling LCS (indicated by the white arrow). This is in contrast to the approach based on FTLE ridge intersection [SW10] (Figure 2(b)), where the extracted HT was repelled from the LCS during its integration (white arrow). Note that the extracted trajectory was repelled although substantial efforts were made to obtain a very accurate seed. Admittedly, however, deviations as in Figure 2(b) may still be tolerable, as long as the HT representation resides in a hyperbolic region (green), because the trajectory is repelled from the repelling LCS but at the same time attracted by the attracting LCS. Hence, as long as the manifold grows to the right side (which also depends on the size of the offset for seeding the space-time streamsurface from the hyperbolic trajectory), this does typically not cause problems (see also Figure 8(b) in the work by Machado et al. [MSE13]).

Figure 2(c) shows the result from our approach without trimming the endpoints of the extracted bifurcation line. Note that, due to the iterative refinement (Section 3.2), a small deformation at the endpoints is produced, which does, however, typically not affect the resulting LCS extraction because the vector field is still hyperbolic along the line and thus attracts the streak manifold.

5.2. Buoyant Barrier Flow

This dataset represents a time-dependent CFD simulation of buoyant air flow in a closed container with a heated bottom, cooled top,

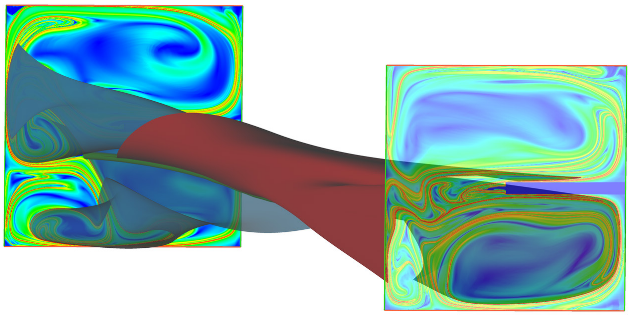

(a)

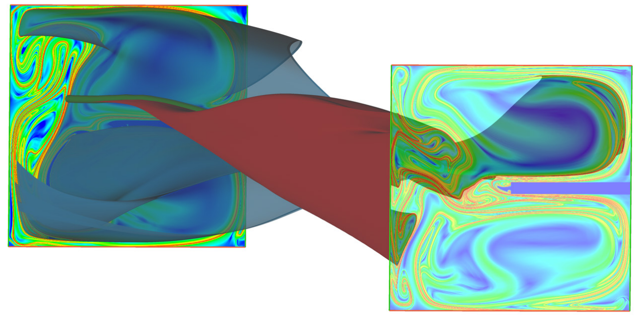

(b)

Figure 3: *Buoyant Barrier Flow dataset. (a) Right FTLE slice: $(t_0, T) = (10.7, 1)$, left slice: $(t_0, T) = (11.5, -1)$. Hyperbolic trajectory by means of space-time bifurcation line (green) and repelling (red) and attracting (blue) LCS by space-time bifurcation manifolds fit well to LCS captured by FTLE ridges. (b) Corresponding visualization with right FTLE slice at $t_0 = 13.7$ and left slice at $t_0 = 14.5$.*

and a horizontal barrier to increase time-dependence. Sadlo and Weiskopf [SW10] visualized the time interval $[2, 2.5]$ with many HTs, both weakly hyperbolic ones and others that gave rise to clear-cut streak manifolds.

Unfortunately, the bifurcation line extraction approach from Machado et al. [MSE13] did not provide space-time bifurcation lines (i.e., hyperbolic trajectories) in this interval. Due to the intricate properties of local feature extraction based on the parallel vectors operator [PR99], we could not identify the reasons why the approach failed. One possible cause is the very low resolution of the vector field (only 40×40 cells compared to 199×199 cells (Oscillating Gyre-Saddle and Quad-Gyre datasets), and 100×100 cells in the Buoyant Plumes dataset (Section 5.3)). Another possible reason is the space-time "velocity" along the space-time bifurcation lines, which might be too low or too high. To demonstrate that our approach works with this data, we selected two time intervals that exhibit pronounced HTs that we could extract with the approach by Machado et al. It is apparent in Figure 3 that our manifolds fit very well to the LCS visualized by the FTLE slices.

5.3. Buoyant Plumes

The last dataset that we apply our technique to was investigated using the FTLE by Bachthaler et al. [BSDW12]. It again represents a CFD simulation of buoyant flow in a closed container, but this time only a small region at the bottom is heated and a small region at the top is cooled. The velocity is initially zero. Two plumes develop, a hot one rising and a cold one dropping. Then, they collide at the center and split into two plumes each, that move horizontally toward the side walls, where they split again. Later, the flow develops asymmetries and finally becomes turbulent.

Figure 4(a) shows the hyperbolic trajectories extracted as space-time bifurcation lines. In Figure 4(b), an early state of the space-time bifurcation manifold computation is shown to illustrate the overall structure of the LCS. The final state is provided in Figure 4(c). We do not visualize the repelling LCS with our technique in this example, because it does not provide significant insight into the dynamics. Our streak manifolds obtained as space-time bifurcation manifolds fit well to the FTLE sections in this example again.

Figure 4(d) shows the same data as Figure 4(c), but from the back for better validation of the manifold with the FTLE. One can see here (and also Figure 1(d) and (e)) that there are FTLE ridge parts that are not captured by a streak manifold. We examine some of these cases in Figure 5 by reverse-time pathlines. In contrast to mapping FTLE to those lines [FSU*10], we color them according to the FTLE value at the respective seed point. It can be seen that whereas FTLE ridges are present in all of the investigated cases, some of the cases lack streak manifolds. The pathline-based inspection reveals that these are cases with weak spread and thus can be considered false positives of the traditional FTLE-based approach.

5.4. Evaluation

The traditional approach to extract LCS, i.e., by computing an FTLE field for each instant of time with subsequent ridge extraction, involves the computation of a large number of pathlines and is therefore an expensive task. The computational cost of such a dense computation, which is also employed by the approach by Bachthaler et al. [BSDW12], scales linearly with resolution, but also with advection time T (number of integration steps). Figure 6(a) provides an analysis with respect to the number of integration steps (observe the increasing cost for ridge extraction due to the growth of LCS). In comparison, our approach (Figure 6(b)) also scales linearly with the number of integration steps, but yields a performance increase of two orders of magnitude compared to the traditional approach, due to its local nature.

Different from the traditional approach, Sadlo and Weiskopf [SW10] need to compute only one forward and one reverse FTLE section at one given time point. The identification of the intersection points between the ridges from these fields then provides the seeds for the integration of hyperbolic trajectories, whose manifolds represent the LCS. Because the FTLE is computed at one section only, this approach is substantially faster. On the other hand, these seeds have to be determined at high accuracy, which is accomplished by adaptive refinement of the FTLE fields. This increases the computational cost (Figure 6(c)), however, it also provides a reduction of the distance between the endpoint of the hyperbolic trajectory and the respective intersection of the LCS at that time point (cf. Figure 2(b)). We use this distance as error measure ε within our

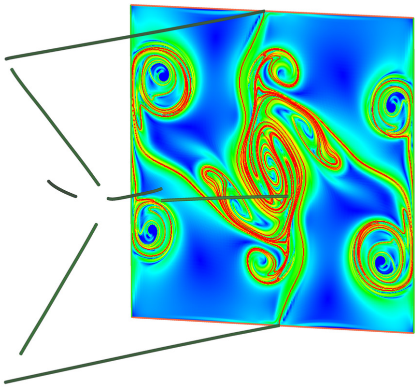

(a)

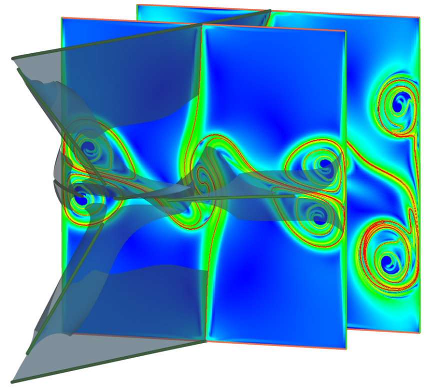

(b)

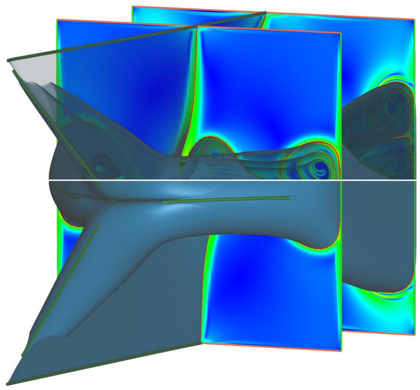

(c)

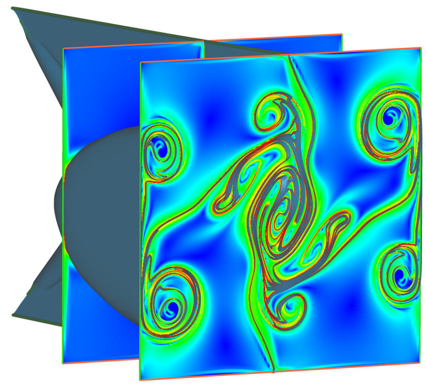

(d)

Figure 4: *Buoyant Plumes dataset in time range $[2.5, 20.1]$, with two FTLE slices with $(t_0, T) = (15, -15)$ and $(20, -20)$. (a) HTs extracted as space-time bifurcation lines (green). (b) Early state of space-time bifurcation manifold integration for better insight into overall structure. (c) Final LCS representation by space-time bifurcation manifolds with transparency in the upper half to reveal internal structure. (d) Same as (c), but from the back for better comparison of FTLE slice and our streak manifolds (see also Figure 1(d) and (e)).*

analysis of the approach by Sadlo and Weiskopf. Please see Figure 6(c) (center and right) for the setups and performance results, and Figure 6(d) for the respective error. Increasing integration time also has a negative impact on accuracy due to error growth. Figure 2(b) shows the result of performing 3500 integration steps. Increasing the resolution alone, without adaptive refinement by subdivision, causes a performance decrease without noticeable gain in accuracy. Our approach, in contrast, is faster and does not exhibit this problem because the HTs are not obtained by integration. Note that all computations, except for Jacobian estimation, were carried out on the GPU.

6. Conclusion

We presented a local extraction approach for hyperbolic trajectories in 2D time-dependent vector fields, providing the time-dependent vector field topology of vector fields without the requirement of computing the FTLE field. In this sense, we provided a true generalization of the traditional vector field topology concept to time-dependent vector fields by conceptually replacing streamlines by streaklines in the original concept and by identifying space-time bifurcation lines as the time-dependent counterpart to saddle-type critical points. We achieved this by extracting bifurcation lines according to Machado et al. [MSE13] from the space-time representation of the vector field. The bifurcation manifolds of these bifurcation lines in the space-time vector field represent the streak manifolds of time-dependent vector field topology, i.e., the attracting and repelling LCS. Besides various advantages, there are also limitations with the current approach, mainly because the bifurcation line extraction technique [MSE13] can miss features and may distort the ends of bifurcation lines. Nevertheless, these issues appear rarely and the deformed ends do typically not affect the result.

The extension of our approach to 3D fields is nontrivial. Üffinger et al. [USE13] have shown that the counterpart to hyperbolic trajectories are hyperbolic pathsurfaces in 3D. Hence, the extension of our method to 3D fields necessitates the extension of bifurcation lines to bifurcation surfaces in 4D space-time, which we plan to pursue as future work.

Acknowledgements

This work was supported by FAPESP (2015/15389-6) and the German Research Foundation within the Cluster of Excellence in Simulation Technology (EXC 310/1).

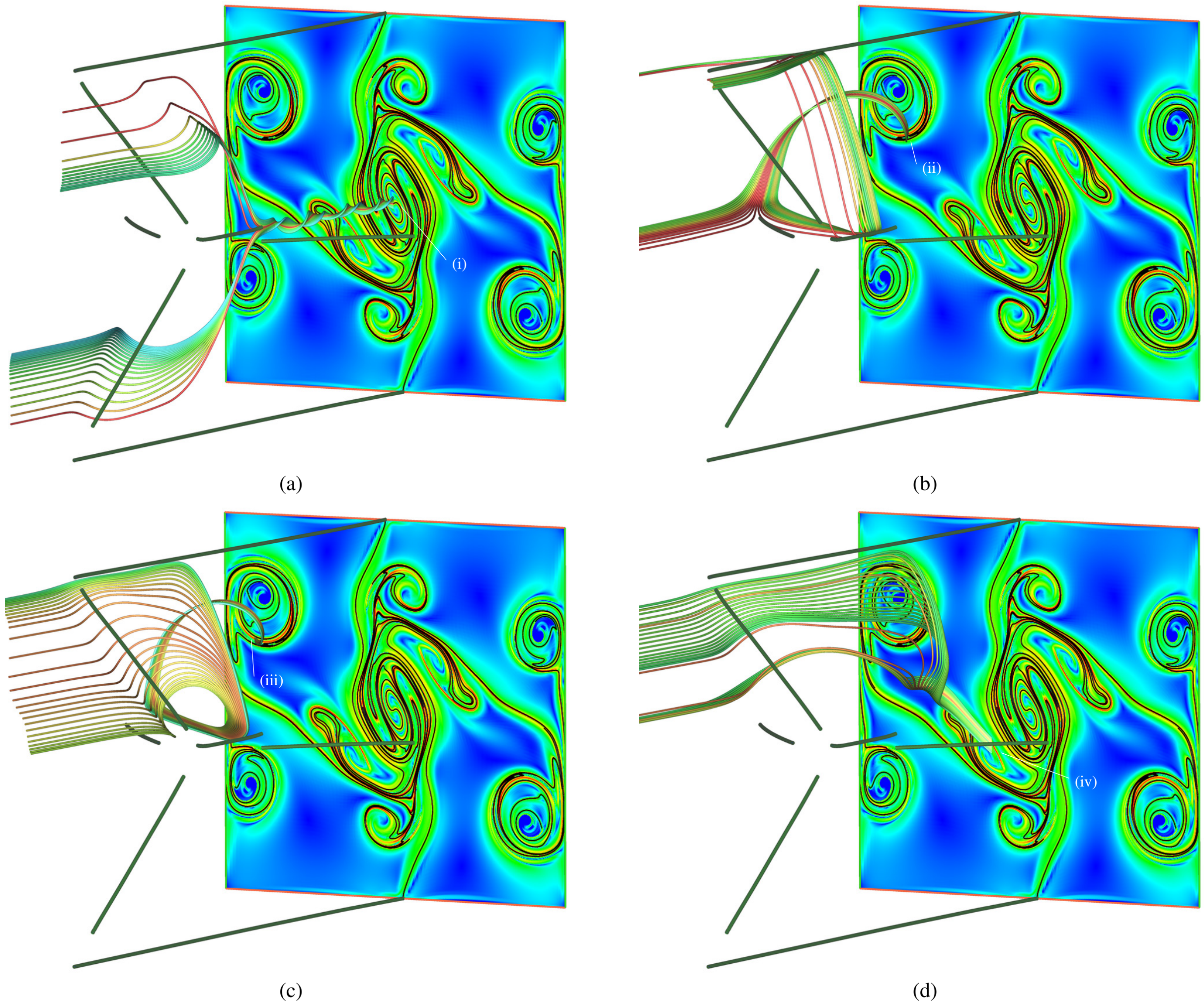

Figure 5: *Relation between streak manifolds (black) and FTLE ridges, by reverse-time pathlines (colors by FTLE), configuration from Figure 4. (a) Very strong spread (diverging red pathlines) with twist, captured by FTLE ridge and streak manifold at (i). (b) Two strong spreads (left and top), captured by FTLE ridge and streak manifold at (ii). (c) Slight divergence of pathlines but no separation, captured by FTLE ridge at (iii) but not by streak manifold. (d) Similar to (c) with stronger divergence, with FTLE ridge at (iv) but no streak manifold. FTLE ridges at (iii) and (iv) can be considered false positives, as indicated by our approach.*

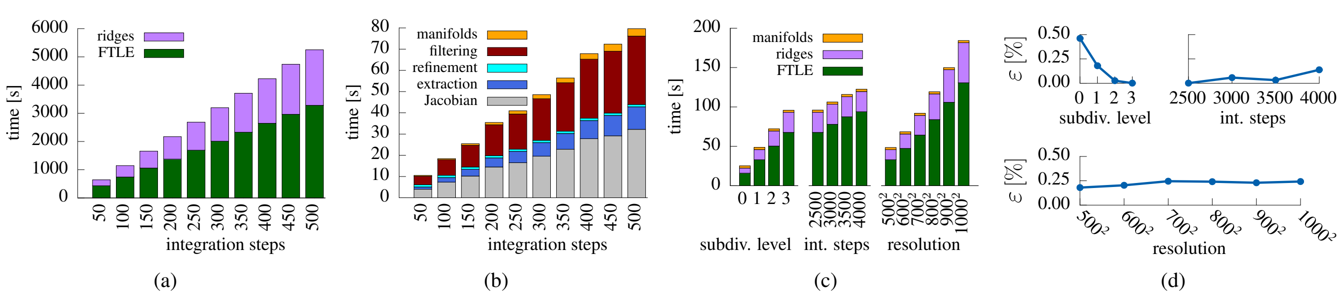

Figure 6: *Comparison of techniques (Oscillating Gyre-Saddle dataset): (a) traditional dense computation (FTLE computation and ridge extraction), (b) our approach (Jacobian estimation, parallel vectors extraction, refinement, filtering, manifold integration), and (c) the approach by Sadlo and Weiskopf (FTLE computation, ridge extraction, manifold integration) for different parameters with (d) respective error ε of the hyperbolic trajectories. Our approach is two orders of magnitude faster than the one based on dense FTLE, and faster than the one by Sadlo and Weiskopf without the issue of deviating HTs due to error growth.*

References

[Asi93] ASIMOV D.: *Notes on the Topology of Vector Fields and Flows*. Tech. Rep. RNR-93-003, NASA Ames Research Center, 1993. 1, 2

[BSDW12] BACHTHALER S., SADLO F., DACHSBACHER C., WEISKOPF D.: Space-time visualization of dynamics in Lagrangian coherent structures of time-dependent 2D vector fields. In *Proc. International Conference on Information Visualization Theory and Applications* (2012), pp. 573–583. 1, 3, 6, 7

[CKW*12] CHEN G., KWATRA V., WEI L.-Y., HANSEN C. D., ZHANG E.: Design of 2d time-varying vector fields. *IEEE Transactions on Visualization and Computer Graphics 18*, 10 (Oct. 2012), 1717–1730. 2

[CL93] CABRAL B., LEEDOM L. C.: Imaging vector fields using line integral convolution. In *Proc. 20th annual conference on Computer graphics and interactive techniques* (1993), SIGGRAPH '93, pp. 263–270. 3

[Ebe96] EBERLY D.: *Ridges in Image and Data Analysis*. Computational Imaging and Vision. Kluwer Academic Publishers, 1996. 1

[FKS*10] FUCHS R., KEMMLER J., SCHINDLER B., SADLO F., HAUSER H., PEIKERT R.: Toward a Lagrangian vector field topology. *Computer Graphics Forum 29*, 3 (2010), 1163–1172. 2

[FSU*10] FALK M., SEIZINGER A., ÜFFINGER M., SADLO F., WEISKOPF D.: Trajectory-augmented visualization of Lagrangian coherent structures in unsteady flow. In *Proc. International Symposium on Flow Visualization* (2010). 7

[GGTH07] GARTH C., GERHARDT F., TRICOCHE X., HAGEN H.: Efficient computation and visualization of coherent structures in fluid flow applications. *IEEE Transactions on Visualization and Computer Graphics 13*, 6 (2007), 1464–71. 1, 2

[Hal00] HALLER G.: Finding finite-time invariant manifolds in two-dimensional velocity fields. *Chaos 10*, 1 (2000), 99–108. 1, 2, 3, 4

[Hal01] HALLER G.: Distinguished material surfaces and coherent structures in three-dimensional fluid flows. *Physica D 149* (2001), 248–277. 1, 2

[Hal11] HALLER G.: A variational theory of hyperbolic Lagrangian coherent structures. *Physica D: Nonlinear Phenomena 240*, 7 (2011), 574–598. 3

[HH89] HELMAN J., HESSELINK L.: Representation and display of vector field topology in fluid flow data sets. *IEEE Computer 22*, 8 (1989), 27–36. 1, 2

[HSW11] HLAWATSCH M., SADLO F., WEISKOPF D.: Hierarchical line integration. *IEEE Transactions on Visualization and Computer Graphics 17*, 8 (2011), 1148–1163. 2

[Ken98] KENWRIGHT D.: Automatic detection of open and closed separation and attachment lines. In *Proc. IEEE Visualization '98* (1998), pp. 151–158. 4

[KHL99] KENWRIGHT D. N., HENZE C., LEVIT C.: Feature extraction of separation and attachment lines. *IEEE Transactions on Visualization and Computer Graphics 5*, 2 (1999), 135–144. 4

[KHNH10] KASTEN J., HOTZ I., NOACK B., HEGE H.-C.: On the extraction of long-living features in unsteady fluid flows. In *Topological Methods in Data Analysis and Visualization. Theory, Algorithms, and Applications*. Springer, 2010, pp. 115–126. 2

[MSE13] MACHADO G. M., SADLO F., ERTL T.: Local extraction of bifurcation lines. In *Proc. International Workshop on Vision, Modeling and Visualization* (2013), pp. 17–24. 2, 3, 4, 5, 6, 7, 8

[PC87] PERRY A. E., CHONG M. S.: A description of eddying motions and flow patterns using critical-point concepts. *Annual Review of Fluid Mechanics 19* (1987), 125–155. 2, 3

[PPF*11] POBITZER A., PEIKERT R., FUCHS R., SCHINDLER B., KUHN A., THEISEL H., MATKOVIC K., HAUSER H.: The state of the art in topology-based visualization of unsteady flow. *Computer Graphics Forum 30*, 6 (2011), 1789–1811. 2

[PR99] PEIKERT R., ROTH M.: The parallel vectors operator: a vector field visualization primitive. In *Proc. IEEE Visualization '99* (1999), pp. 263–270. 4, 5, 7

[Rot00] ROTH M.: *Automatic extraction of vortex core lines and other line-type features for scientific visualization*. PhD thesis, ETH Zurich, No. 13673, 2000. 4

[RP98] ROTH M., PEIKERT R.: A higher-order method for finding vortex core lines. In *Proc. IEEE Visualization '98* (1998), pp. 143–150. 4, 6

[Sad15] SADLO F.: Lyapunov time for 2D Lagrangian visualization. In *Topological and Statistical Methods for Complex Data*. Springer Berlin Heidelberg, 2015, pp. 167–181. 2

[SBDW13] SADLO F., BACHTHALER S., DACHSBACHER C., WEISKOPF D.: Space-time flow visualization of dynamics in 2D Lagrangian coherent structures. In *Computer Vision, Imaging and Computer Graphics. Theory and Application*. Springer Berlin Heidelberg, 2013, pp. 145–159. 1

[SH95] SUJUDI D., HAIMES R.: Identification of swirling flow in 3D vector fields. In *Proc. 12th AIAA Computational Fluid Dynamics Conference* (1995), pp. 95–1715. 4, 6

[SLM05] SHADDEN S., LEKIEN F., MARSDEN J.: Definition and properties of Lagrangian coherent structures from finite-time lyapunov exponents in two-dimensional aperiodic flows. *Physica D: Nonlinear Phenomena 212*, 3-4 (2005), 271–304. 1, 2, 3

[SP07] SADLO F., PEIKERT R.: Efficient visualization of Lagrangian coherent structures by filtered AMR ridge extraction. *IEEE Transactions on Visualization and Computer Graphics 13*, 5 (2007), 1456–1463. 1, 2

[SPFT12] SCHINDLER B., PEIKERT R., FUCHS R., THEISEL H.: Ridge concepts for the visualization of Lagrangian coherent structures. In *Topological Methods in Data Analysis and Visualization II* (2012), Springer, pp. 221–235. 1

[SRP11] SADLO F., RIGAZZI A., PEIKERT R.: Time-dependent visualization of Lagrangian coherent structures by grid advection. In *Topological Methods in Data Analysis and Visualization* (2011), Springer, pp. 151–165. 1, 2

[SUEW12] SADLO F., ÜFFINGER M., ERTL T., WEISKOPF D.: On the finite-time scope for computing Lagrangian coherent structures from Lyapunov exponents. In *Topological Methods in Data Analysis and Visualization II*. Springer, 2012, pp. 269–281. 2

[SW10] SADLO F., WEISKOPF D.: Time-dependent 2-D vector field topology: An approach inspired by Lagrangian coherent structures. *Computer Graphics Forum 29*, 1 (2010), 88–100. 1, 2, 3, 4, 5, 6, 7

[TGS05] TRICOCHE X., GARTH C., SCHEUERMANN G.: Fast and robust extraction of separation line features. In *Scientific Visualization: The Visual Extraction of Knowledge from Data* (2005), Springer, pp. 249–264. 4

[TS03] THEISEL H., SEIDEL H.-P.: Feature flow fields. In *Proc. Symposium on Data visualisation 2003* (2003), pp. 141–148. 2

[TWHS04] THEISEL H., WEINKAUF T., HEGE H.-C., SEIDEL H.-P.: Stream line and path line oriented topology for 2D time-dependent vector fields. In *Proc. IEEE Visualization '04* (2004), pp. 321–328. 2

[USE13] ÜFFINGER M., SADLO F., ERTL T.: A time-dependent vector field topology based on streak surfaces. *IEEE Transactions on Visualization and Computer Graphics 19*, 3 (2013), 379–392. 1, 2, 3, 4, 5, 8

[USK*12] ÜFFINGER M., SADLO F., KIRBY M., HANSEN C., ERTL T.: FTLE computation beyond first-order approximation. In *Short Paper Proc. Eurographics 2012* (2012), pp. 61–64. 2

[WT10] WEINKAUF T., THEISEL H.: Streak lines as tangent curves of a derived vector field. *IEEE Transactions on Visualization and Computer Graphics 16*, 6 (2010), 1225–1234. 4

[WTS*07] WIEBEL A., TRICOCHE X., SCHNEIDER D., JAENICKE H., SCHEUERMANN G.: Generalized streak lines: Analysis and visualization of boundary induced vortices. *IEEE Transactions on Visualization and Computer Graphics 13*, 6 (2007), 1735–1742. 3